# Zomin, Uzbekistan: A Spatial–Ecological Sustainability Index

**Botirjon Karimov[1,*], Ziyodulla Khakimov[2], Shirin Karimova[3]**
[1]University of Tasmania, Hobart, Australia
[2]Alfraganus University, Tashkent, Uzbekistan
[3]Tashkent State University of Economics, Tashkent, Uzbekistan
Emails: botirjon.karimov@utas.edu.au; z.xakimov@afu.uz; karimovashirin22@gmail.com

**Abstract**

Arid and semi-arid regions are facing faster land degradation and growing water stress. Planners need indicators that connect conservation goals to everyday decisions. In Uzbekistan's Zomin region, few long-term, spatial studies combine vegetation condition with water-conservation capacity. We develop a transparent Spatial–Ecological Sustainability Index (SESI) to describe ecological quality and water support and to guide restoration and protection. The method merges several remote sensing and GIS layers: multi-decade NDVI from Landsat and Sentinel, terrain measures such as slope and flow accumulation, and land-cover permeability. We normalize these layers and combine them with a tested weighting method, producing SESI maps and summaries for districts and protected areas. The results show clear patterns by elevation and land use: upper catchments have strong water-retention potential, while valley bottoms near settlements show mixed conditions. The approach is reproducible, decision-ready, and adaptable to other mountainous, water-limited regions.

**Keywords:** Zomin; NDVI; GIS; Spatial data fusion; Remote sensing; Desertification; Ecotourism; YOLOv11

## 1. Introduction

Ecological restoration and environmental management of mines have become a major global priority [1]. Mining relics, which are unique traces of human alteration of nature, can be repurposed as public parks through careful landscape redesign [2]. This study proposes an integrated method to compute a Social Development Status Index for regional planning. The method links environmental conservation with practical decision-making. Evaluating the region's geography through its resource base is important. Water use, in particular, affects settlements, ecosystems, and habitat quality. Evaluating the region's geography through its resource base is important. Water use, in particular, affects settlements, ecosystems, and habitat quality [3]. Research on changes in ecological quality and water-conservation capacity in tertiary conservation areas is common today [4]. However, in Uzbekistan the Zomin region has been studied only rarely. Our work analyzes about 40 years of satellite imagery to fill this gap [5].

Arid and semi-arid lands are eco-sensitive environments with minimal water resources and sparse vegetation cover [6]. This makes long-term ecological monitoring crucial in regions like Zomin, Uzbekistan, which have historically lacked continuous study. Here, we present a multi-decadal remote sensing analysis of ecological quality (vegetation condition) and water conservation capacity in the Zomin region by leveraging 40 years of satellite imagery. Satellite-based observations and GIS tools enable the tracking of vegetation health and hydrological trends over broad spatial scales. In particular, the Normalized Difference Vegetation Index (NDVI) has become one of the most widely used metrics for quantifying vegetation greenness and ecosystem health from space [7]. Time-series NDVI data serve as an indicator of vegetation dynamics and have been linked to changes in water availability and drought impacts [8]. By examining four decades of NDVI and related indices, we infer long-term trends in plant productivity, moisture status, and the efficacy of natural water conservation (e.g. soil moisture retention) in the landscape. Long-term studies of this kind are rare in Zomin, making our analysis an important baseline for the region. Such data-driven insights are vital for guiding ecological restoration efforts and conservation planning, as they provide *in situ*-scaled information for environmental protection and resource management in arid environments[9]. Furthermore,



DOI: https://doi.org/10.54216/JIER.010102
Received: December 14, 2024 Revised: January 23, 2025 Accepted: February 25, 2025

recent advances in remote sensing analytics enhance monitoring precision. Deep learning models like YOLO (You Only Look Once) now enable automatic detection of environmental features in high-resolution imagery, and the integration of multi-source data fusion has improved the comprehensiveness of monitoring[10]. By combining traditional NDVI-based assessments with these emerging tools, this study achieves a more accurate and comprehensive evaluation of vegetation health and water trends, informing sustainable ecosystem management in arid and semi-arid regions. We apply NDVI, GIS mapping, spatial data fusion, and a deep-learning detector such as YOLOv11 to identify ecological change. Vegetation trends plus surface-water dynamics are tracked to support sustainable actions. The case study focuses on Zomin National Park with emphasis on biodiversity protection and desertification control. Findings indicate a need to balance environmental safeguards with tourism development to secure long-term ecological as well as economic benefits.

## 2. Study area

This study focuses on Zomin District in the Jizzakh Region of Uzbekistan (see Figure 1). Over the past 35 years (1990–2024), the area has experienced noticeable climatic shifts consistent with regional warming and greater hydro-climatic variability. These changes appear as fluctuations in open-water extent, vegetation condition, and localized drought stress.

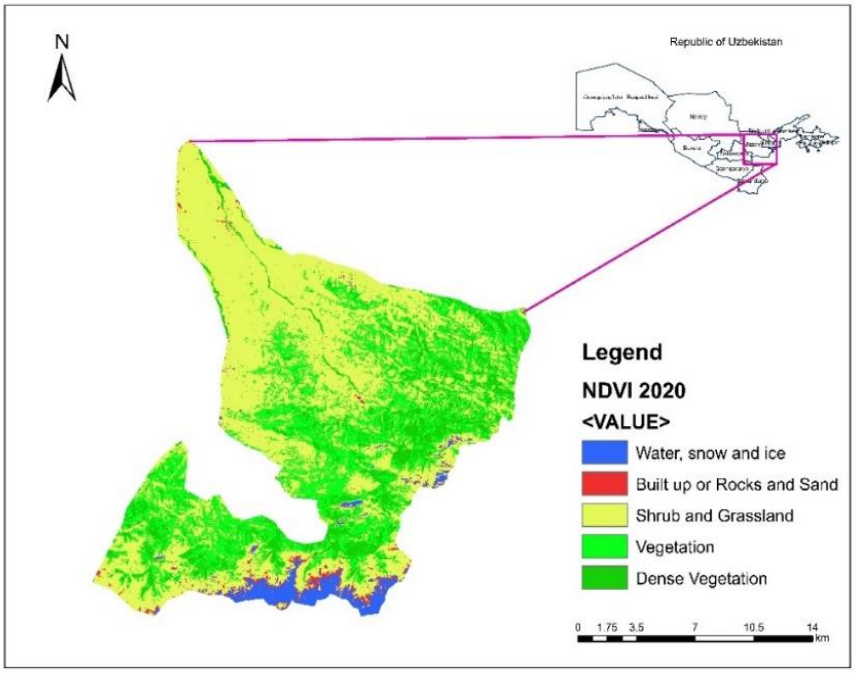


**Figure 1.** Spatial Distribution of Vegetation Density in Zomin, Jizzakh Region, Uzbekistan

Using GIS and multi-sensor remote sensing, we characterize key environmental features of the region, including topography, surface water bodies, and land-surface moisture. This provides a reproducible baseline for monitoring water resources and detecting drying hotspots, while placing patterns in their hydrological context (e.g., flow-accumulation pathways and potential bottlenecks). Within this project, we map annual and seasonal patterns of open water using NDWI/MNDWI, assess surface moisture and drought using NDMI/NDDI, and quantify changes over time (km², %) for 1990–2024. The outputs highlight priority zones for monitoring, maintenance, and future field verification, and establish the geographic frame used throughout the analysis.

## 3. Materials and Methods

### 3.1 Dataset

The Normalized Difference Vegetation Index (NDVI) is a widely used vegetation index because of its simplicity, ease of application, and broad familiarity. Time-series NDVI products derived from multiple satellite sensors, such as NOAA/AVHRR (Advanced Very High Resolution Radiometer), MODIS (Moderate Resolution Imaging Spectroradiometer), Landsat TM (Thematic Mapper), ETM+ (Enhanced Thematic Mapper Plus), and SPOT/VEGETATION, are powerful tools for reconstructing past conditions, monitoring current natural-resource status and long-term land-use and land-cover change, and extracting canopy biophysical and phenological information. These products are also used to forecast trends in terrestrial ecosystems at global, continental, and regional scales [11]. However, NDVI time series remain spatio-temporally discontinuous because of cloud cover,



DOI: https://doi.org/10.54216/JIER.010102
Received: December 14, 2024 Revised: January 23, 2025 Accepted: February 25, 2025

seasonal snow, atmospheric variability, bidirectional reflectance effects, and instrument issues [12]. Such biases can limit NDVI's effectiveness for vegetation-dynamics monitoring and global-change research. NDVI is computed as:

$$NDVI = \frac{NIR-RED}{NIR+RED} \quad (1)$$

In the context of satellite imagery, NIR and RED refer to the spectral information that is captured by sensors integrated on the satellite. Radiance (W*cdotpsr* $^{-1}$ ·m$^{-2}$ ·μm$^{-1}$) is the measure of energy flux recorded by a sensor. These values are often rescaled to digital numbers (DN) in 16-bit, 8-bit, and 12-bit integers see Formula 1. Reflectance is unitless measure of the ratio of radiation reflected by an object relative to the radiation incident upon the object. The NDVI value varies from -1 to 1. Higher the value of NDVI reflects high Near Infrared (NIR), which means dense greenery. Generally, we obtain following results:

- NDVI = -1 to 0 represent Water bodies
- NDVI = -0.1 to 0.1 represent Barren rocks, sand, or snow
- NDVI = 0.2 to 0.5 represent Shrubs and grasslands or senescing crops
- NDVI = 0.6 to 1.0 represent Dense vegetation or tropical rainforest

Data and Methods. In this study, Landsat imagery for 1990, 2000, 2010, 2020, and 2024 was obtained from [13]. The Landsat missions consist of Earth-observing satellites operated under the U.S. Geological Survey (USGS) National Land Imaging (NLI) Program. Products generated from Landsat sensors are curated and distributed by the USGS Earth Resources Observation and Science (EROS) Center in Sioux Falls, South Dakota. For preprocessing, the selected scenes were imported into ArcMap 10.5.1, stacked as multilayer rasters, and mosaicked to create seamless coverage of the study area. The workflow included scene selection, layer stacking, mosaicking, and preparation of analysis-ready composites.

1. Open ArcToolbox
2. Data Management Tool
3. Raster
4. Raster Dataset

After preparing the mosaic layers, we imported them into the GIS environment to compute the Normalized Difference Vegetation Index (NDVI). NDVI values were calculated for 1990, 2000, 2010, 2020, and 2024. For 1990–2010, we used Landsat 5 imagery; for subsequent years, we used data from other Landsat missions (e.g., Landsat 7/8/9) when available to maintain continuity of the vegetation-index time series. This approach applies to NDVI to monitor vegetation conditions and to support ecological assessment at regional and broader scales.

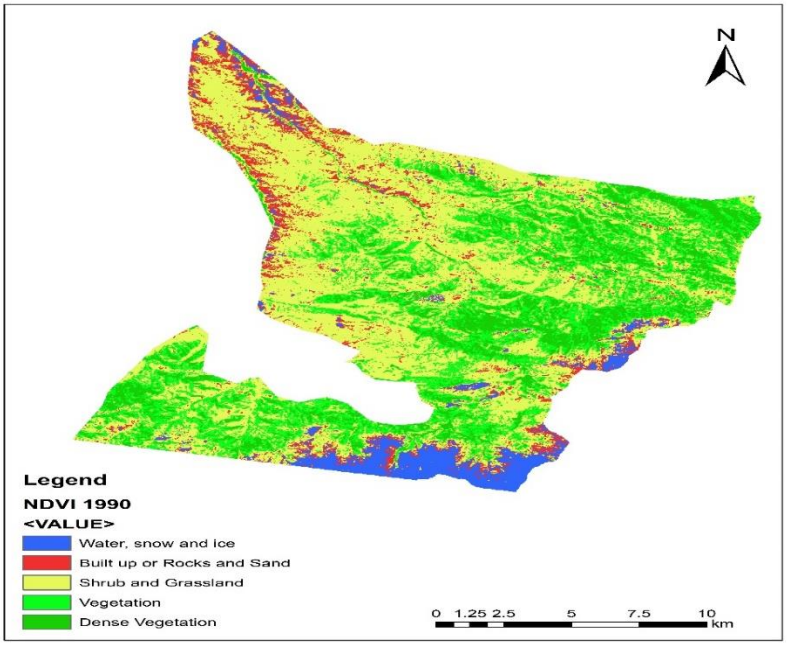


**Figure 2a.** NDVI for the year **1990**



DOI: https://doi.org/10.54216/JIER.010102
Received: December 14, 2024 Revised: January 23, 2025 Accepted: February 25, 2025

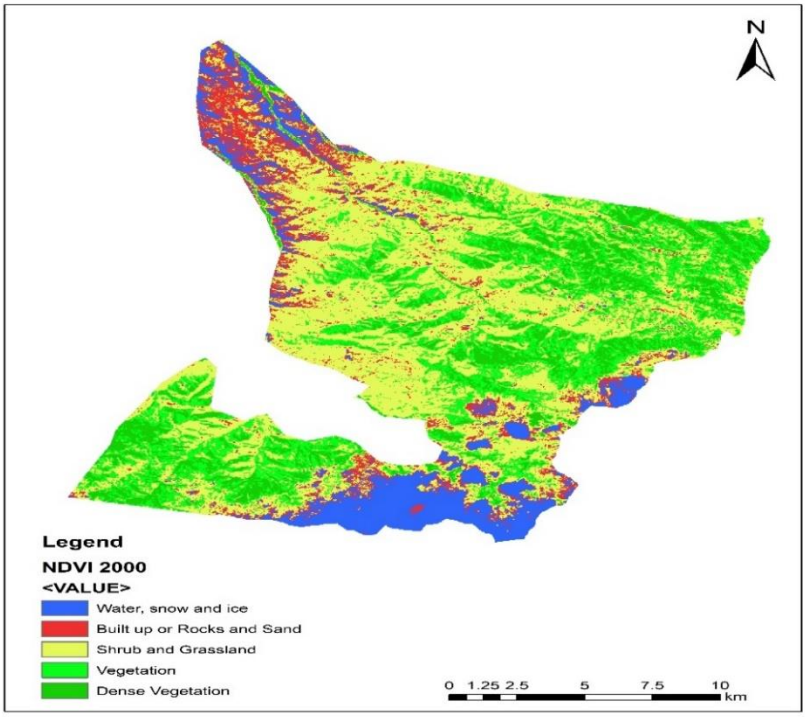


**Figure 2b.** NDVI for the year **2000**

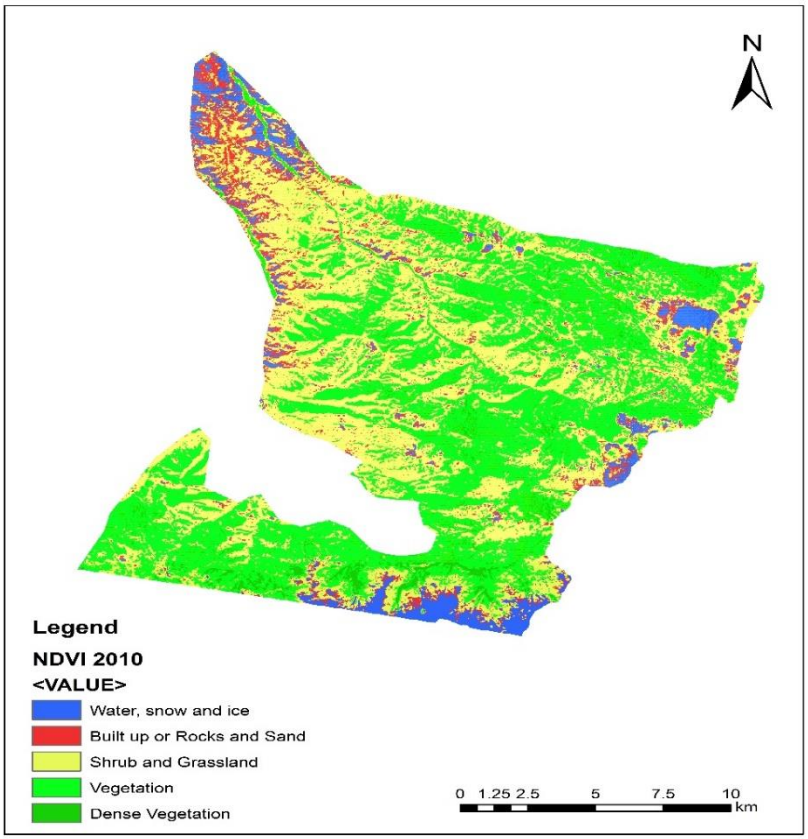


**Figure 2c.** NDVI for the year **2010**



DOI: https://doi.org/10.54216/JIER.010102
Received: December 14, 2024 Revised: January 23, 2025 Accepted: February 25, 2025

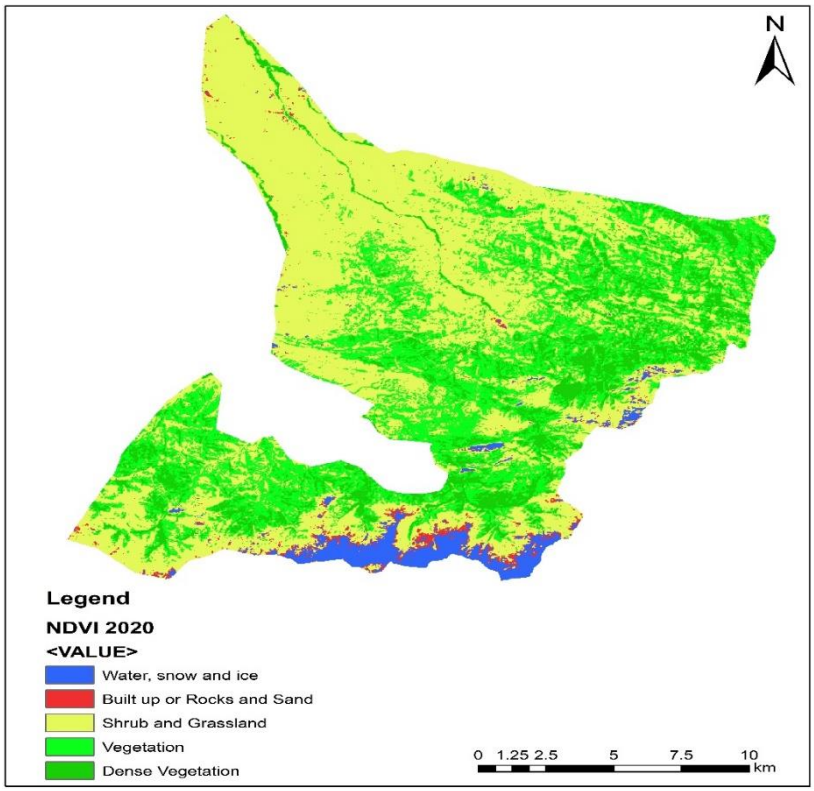


**Figure 2d.** NDVI for the year **2020**

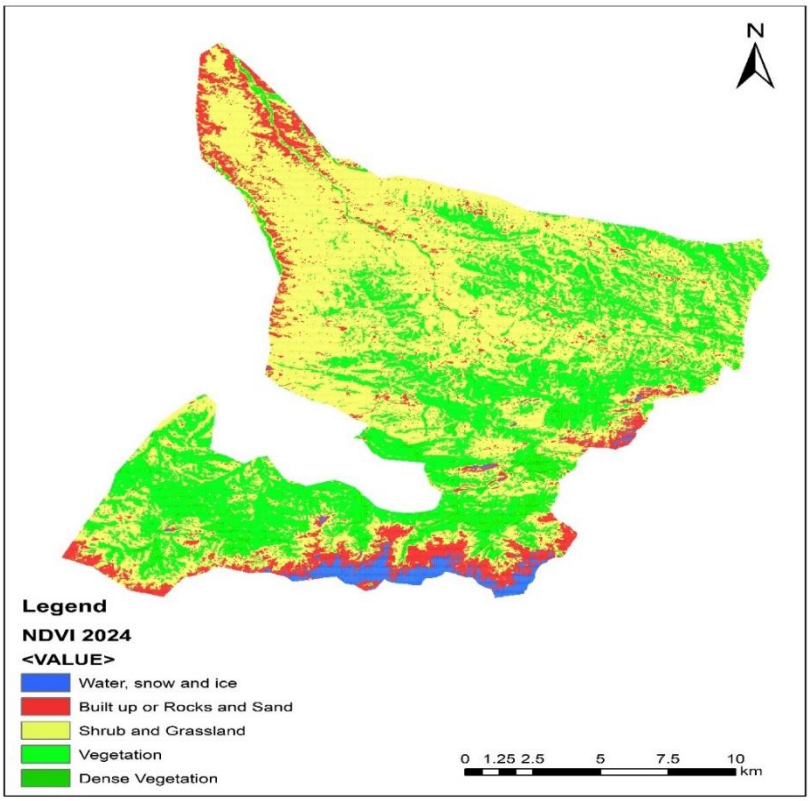


**Figure 2e.** NDVI for the year **2024**



DOI: https://doi.org/10.54216/JIER.010102
Received: December 14, 2024 Revised: January 23, 2025 Accepted: February 25, 2025

Results and Visualization. Based on the NDVI calculations, Figures 2a–2d show maps for 1990, 2000, 2010, and 2020. The maps reveal changes in vegetation greenness over time, highlighting trends across the study area. To combine data from different satellites, we used spatial data fusion. This step aligns spectral inputs, spatial resolution, and acquisition dates, which improves temporal consistency. We then estimated ecological metrics more accurately by pairing the NDVI series with GIS layers. Where useful, we also applied a deep-learning tool (YOLOv11) to flag local anomalies.

3.2 Development Phase

This section outlines the development phase for our initial research work. First, we assembled satellite and GIS imagery covering roughly two decades, then applied color thresholding to map drought-affected zones. This screening helps decision makers who need clear separation between vegetated and barren areas for policy design. We focused on the Zomin region (see Figure 1) to assess its ecological status. Time-series observation is essential for tracking green areas over time. Accordingly, we used Landsat 5 for 1990, 2000, and 2010, plus Landsat 8 for 2020. All scenes were georeferenced to 2047 columns by 1527 rows to support consistent spatial analysis. We generated masks with color thresholding, then applied modern deep-learning methods to locate dense foliage, arid zones, or other priority features. As shown in Figure 3, we use YOLOv11, a fast real-time object detector from the current state of the art [14]. This configuration lets us classify vegetation versus drought-affected regions in large image sets with high speed and strong efficiency [15]. The throughput suits long time-series archives, which enables near-real-time analysis in future deployments.

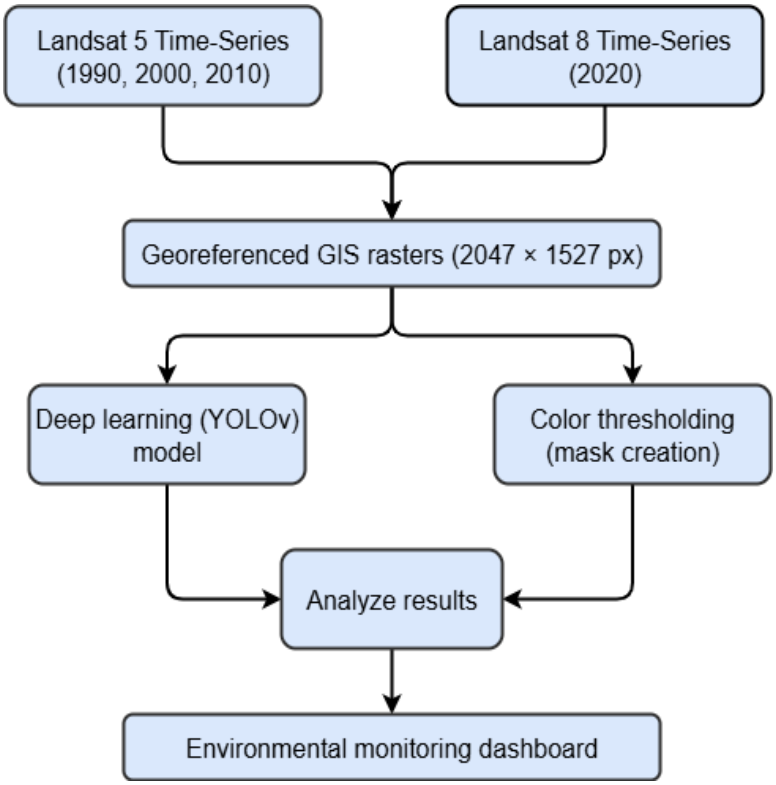


**Figure 3.** Workflow for the ecotourism recommendation engine using GIS data and a deep-learning model

Rising desertification poses new challenges for Zomin. Comparing vegetation cover and surface-water layers for 1990 and 2024 reveals shifts consistent with increasing aridity. We use NDVI-based vegetation maps plus water masks to quantify these changes, flag drying hotspots, and set priorities for follow-up analysis. Future work will extend to change detection, land-cover classification, building extraction, road extraction, urban-area mapping, and vehicle detection using remote-sensing imagery. We also evaluate YOLOv11 together with color thresholding on the Zomin archive to produce timely risk layers.

3.3 Color Thresholding (Mask Creation)

Color thresholding is a key step for creating masks in this study, because the GIS imagery lets us distinguish vegetation from drought-affected areas. We set limits on standard color channels to select target classes (for



DOI: https://doi.org/10.54216/JIER.010102
Received: December 14, 2024 Revised: January 23, 2025 Accepted: February 25, 2025

example, green for vegetation or red for arid ground). This segmentation lets us estimate the area of each ecological zone and track changes over time. For each image (NDVI-derived or RGB), we define bounds per channel and test every pixel against those bounds to build a binary mask. Formally, for a pixel $p(x, y)$ with channels R,G,B. $M(x, y)$ is based on thresholds for each color channel:

$$M_{green}(x,y) = \begin{cases} 1 \; if \; R_{min} \le R(x,y) \le R_{max} \; and \; G_{min} \le G(x,y) \le G_{max} \; and \; B_{min} \le B(x,y) \le B_{max} \\ 0 \; otherwise \end{cases}$$

(2)

Where:

- $R(x, y), G\ (x, y),$ and $B(x, y)$ are the red, green, and blue channel values at pixel $(x, y)$.
- $R_{min,}\ R_{max,}\ G_{min,}\ G_{max,}\ B_{min,}\ B_{max,}$ are the threshold values defining the range for green or red areas.

In Formula 2, creates a binary mask $M_{green}\ (for\ green) and\ similarly\ M_{red}$ for red, where pixels within the threshold range are marked as 1 (indicating the belong to that class), and others are marked as 0. Then pixel-to-distance scale calculation on the images (see Figure 2a, b, c, and d: NDVI Analysis for Zomin National Park Across Four Time Periods) indicates distances in kilometers. From the scale bar at the bottom, it appears to cover distances up to 12 kilometers. Given that the image width is 2047 pixels and the scale bar indicates 12 kilometers, we can calculate the pixel-to-distance scale as follows:

$$Distance\ per\ pixel = \frac{12\ km}{2047\ pixels} \approx 0.00586\ \text{km/pixel}$$

(or approximately 5.86 meters per pixel) Each pixel represents approximately 5.86 meters in real-world distance, yielding a pixel resolution for the image. To calculate the percentage of green or red areas in an image, divide the number of pixels belonging to that class by the total number of pixels in the image. For a binary $M$ (where 1 represents the class of interest, such as green areas), the formula 3 for the percentage of green pixels is:

$$Green\ Percentage = \frac{\sum M_{green}\ (x,y)}{Total\ Pixels} \times 100 \qquad (3)$$

Where:

- $\sum M_{green}\ (x, y)$is the count of green pixels (i.e., where $M_{green}\ (x, y) = 1$).
- *Total Pixels = Image Width × Image Height.*

This gives the proportion of green or red areas as a percentage of the total area. These formulas (2,3) form the mathematical basis of your current NDVI analysis using rule-based color thresholding and can also be used if ground truth data is available for accuracy assessment. Let me know if you'd like more detailed formulas or additional metrics! Now, we can see in Figure 3 the results of several images, labeled as a, b, c, d, e, f, h, l, and m.

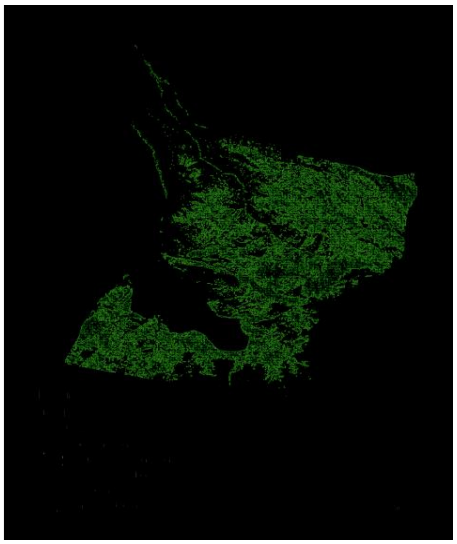

(a) 1990

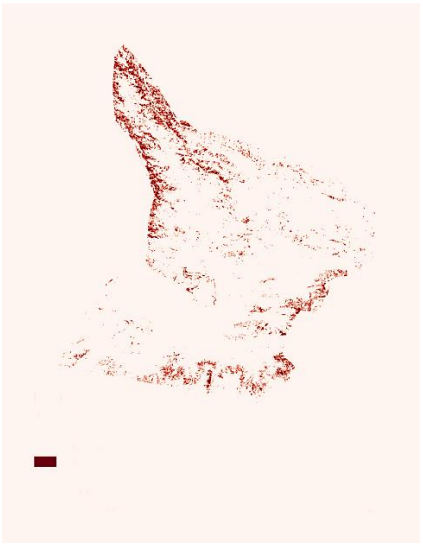

(b) 1990



DOI: https://doi.org/10.54216/JIER.010102
Received: December 14, 2024 Revised: January 23, 2025 Accepted: February 25, 2025

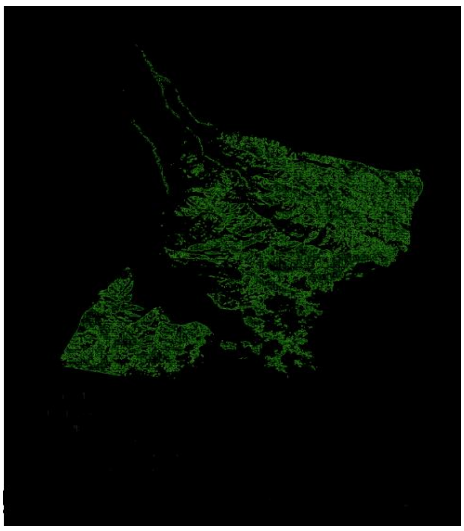

(c) 2000

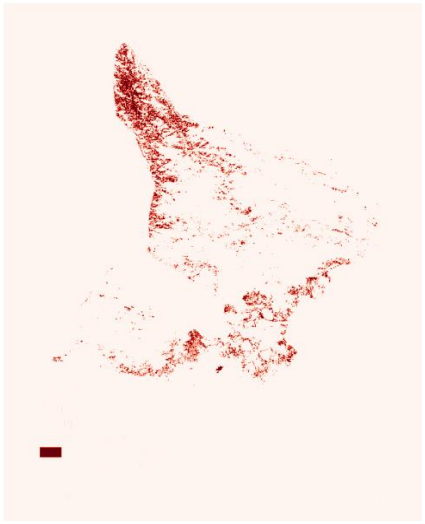

(d) 2000

(e) 2010

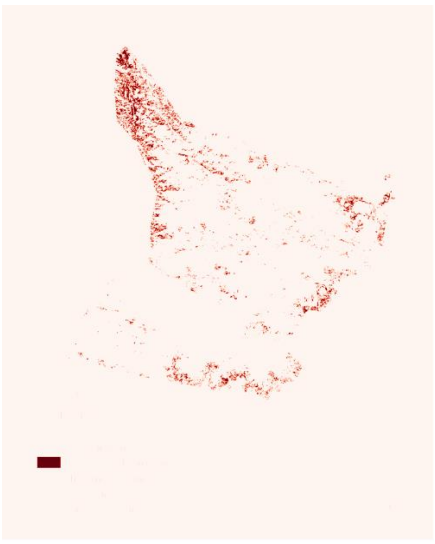

(f) 2010

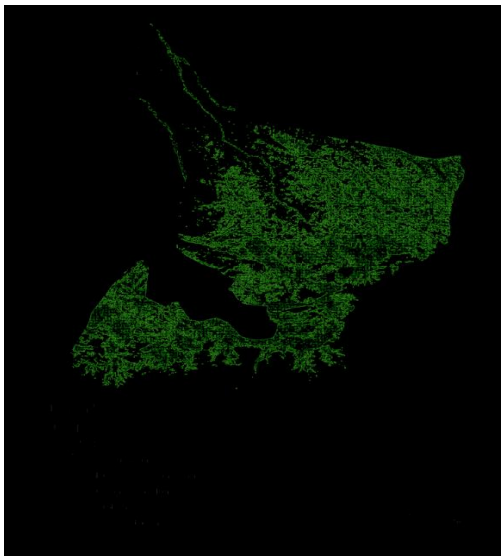

(g) 2020

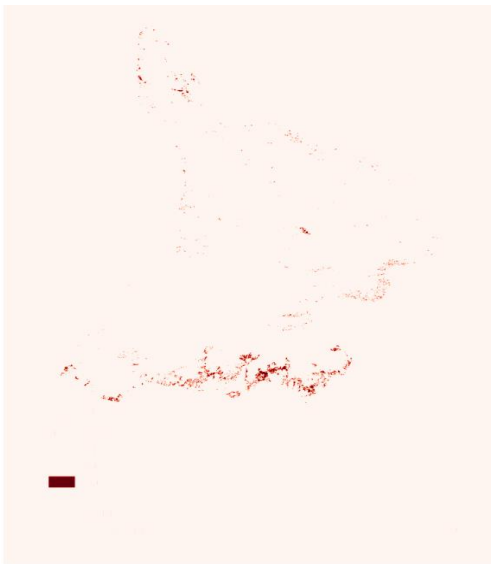

(h) 2020



DOI: https://doi.org/10.54216/JIER.010102
Received: December 14, 2024 Revised: January 23, 2025 Accepted: February 25, 2025

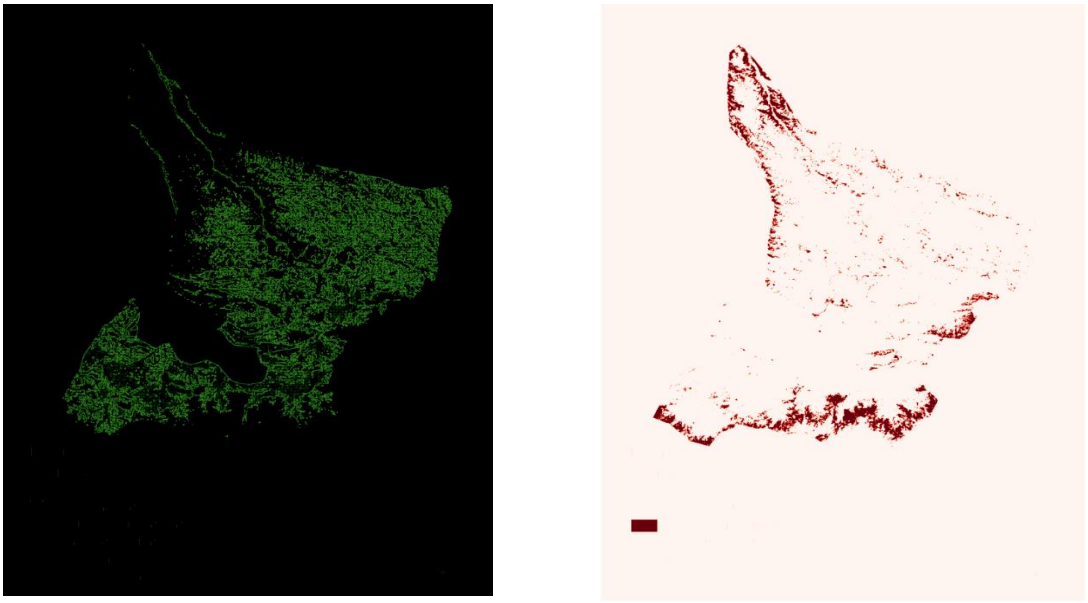

(i) 2010 (j) 2010

**Figure 3.** Contrast iomages for duuring 2 decades int chanches of the climate condition for the area

In this study (see Figure 3), we performed land-cover classification on satellite imagery from 1990 to 2024. The segmentation separated vegetation, buildings, rocks, and sand (non-vegetated or sparsely vegetated areas). This semantic segmentation enabled precise separation of landscape types. Vegetation pixels were shown on a black background, while buildings, rocks, and sand were shown on a white background. The high contrast made changes easy to see. The segmented outputs achieved high visual clarity and improved the display of temporal change in the classification results.

3.4 Deep learning methodologies

We use the recent YOLOv11 model for real-time object detection to support environmental monitoring [16]. YOLOv11 is a fast one-stage detector that keeps high detection accuracy. The model scales to large image archives and enables precise spatial analysis on high-resolution scenes. In a single pass, YOLOv11 processes an image and outputs multiple bounding boxes with class probabilities [17]. This one-pass design differs from multi-stage pipelines, which gives an advantage for real-time tasks in environmental monitoring. The model divides the image into a fixed grid. Each grid cell is responsible for detecting objects whose centers fall inside that cell. Convolution layers extract spatial features from the input. The resulting feature map is split into grid cells. Each cell predicts box coordinates ($x$,$y$,$w$,$h$) and class probabilities. Predictions are refined with anchor boxes to better match object shapes. Each bounding box also receives an objectness score. The final confidence for a class equals objectness multiplied by the class probability. This setup supports fast screening of large datasets while keeping accuracy high.

$$\textit{Confidence Score} = P(\textit{object}) \times IOU_{\text{pred, truth}} \quad (4)$$

where $P(\textit{object})$ represents the probability of an object's presence, and $IOU_{\text{pred, truth}}$, truth (Intersection over Union) measures the overlap between the predicted bounding box and the ground-truth box Formula 4. The YOLOv11 model uses anchor-based bounding box prediction, refined through the following transformations:

$$\hat{x}=\sigma(t_x) + c_x \quad (5)$$

$$\hat{y}=\sigma(t_y) + c_y$$

$$\hat{w}=p_w \ e^{t_w}$$

$$\hat{h}=p_h \ e^{t_h}$$

where:

- $(c_y, c_y)$ represents the grid cell coordinates,
- $p_{w,}\ p_h$ are the anchor box dimensions,
- and $\sigma$ denotes the sigmoid function, bounding $t_x$ and $t_y$ within [0,1] for cell-specific predictions in the Formula 5.



DOI: https://doi.org/10.54216/JIER.010102
Received: December 14, 2024 Revised: January 23, 2025 Accepted: February 25, 2025

We have developed YOLOv11 into the workflow to separate water bodies and vegetation in the study area. The model detects ecological features at high speed with strong accuracy. It also helps map the spatial relationship between water and green cover. These outputs feed the GIS layers used for monitoring and risk screening. With this specificity, we can flag segments that show water loss or vegetation decline. The system supports prioritization of sites for maintenance, restoration, or field checks. In our pipeline, YOLOv11 serves as a core component that scales to large image archives and sustains near–real-time updates.

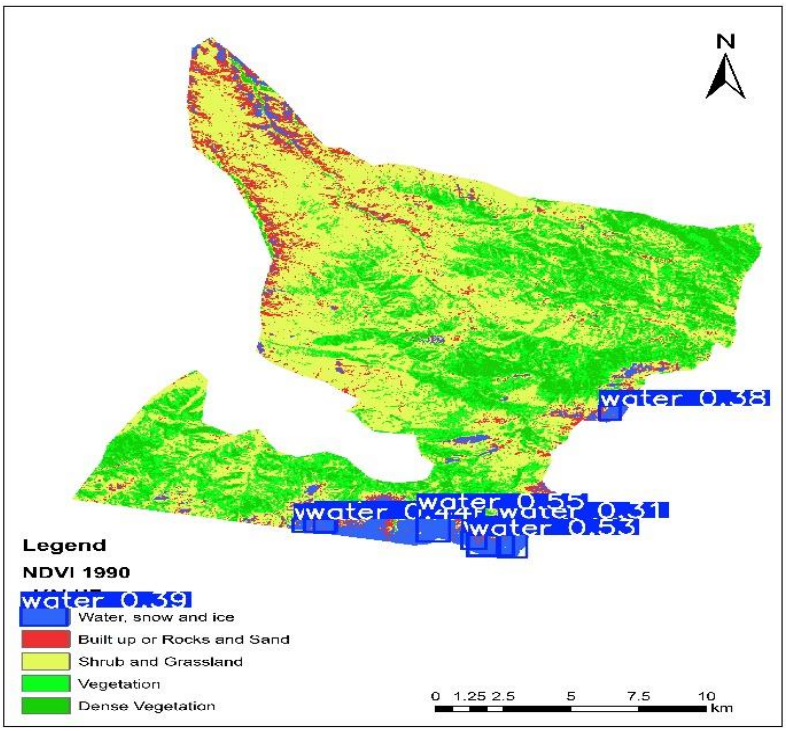


**Figure 4.** (*a) Detection results for the year 1990*

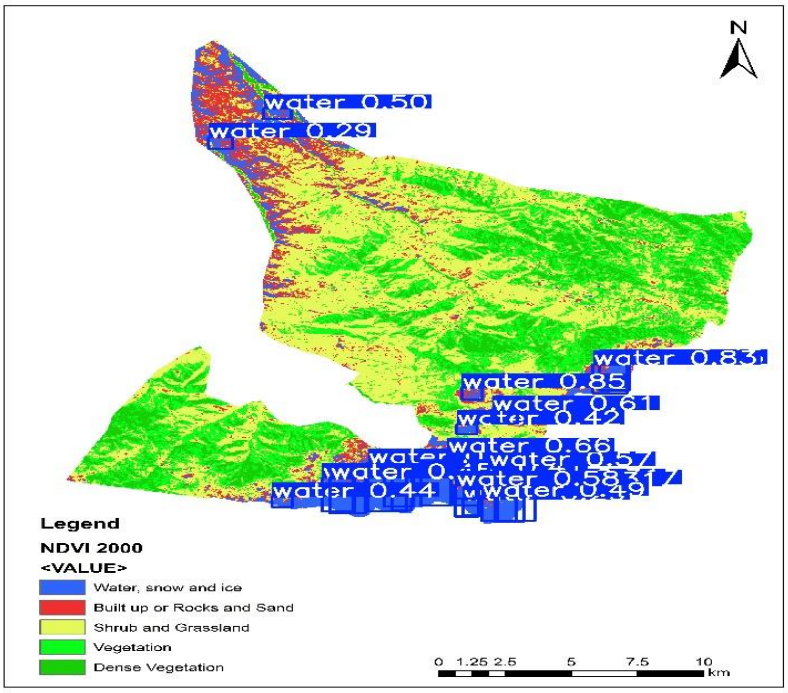


**Figure 4.** *(b) Detection results for the year 2000*



DOI: https://doi.org/10.54216/JIER.010102
Received: December 14, 2024 Revised: January 23, 2025 Accepted: February 25, 2025

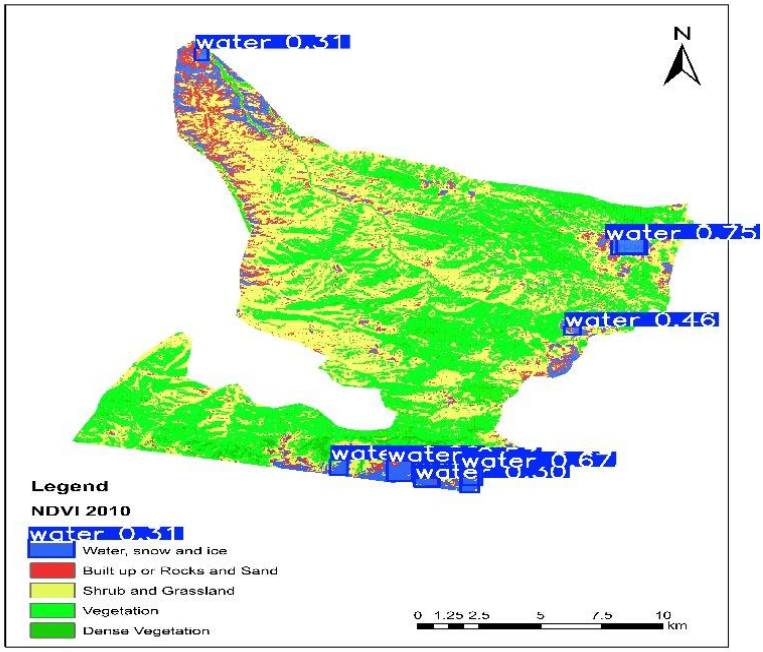


**Figure 4.** *(c) Detection results for the year 2010*

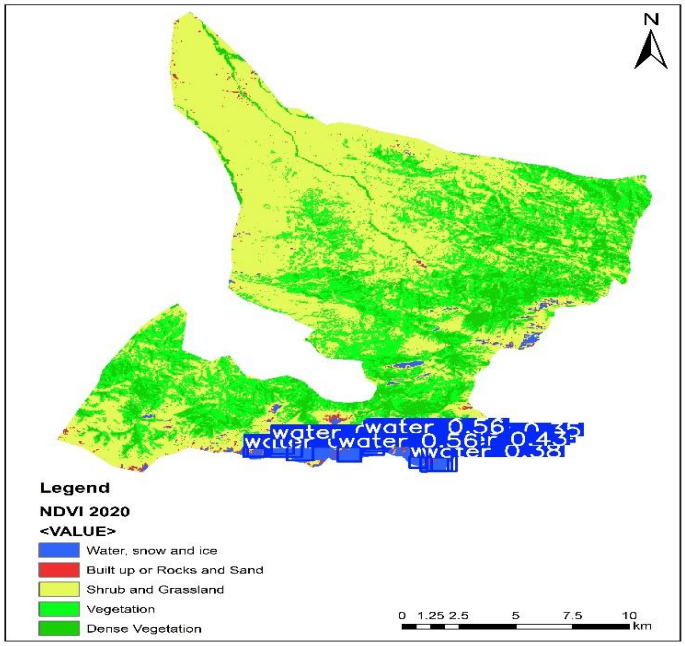


**Figure 4.** *(d) Detection results for the year 2020*



DOI: https://doi.org/10.54216/JIER.010102
Received: December 14, 2024 Revised: January 23, 2025 Accepted: February 25, 2025

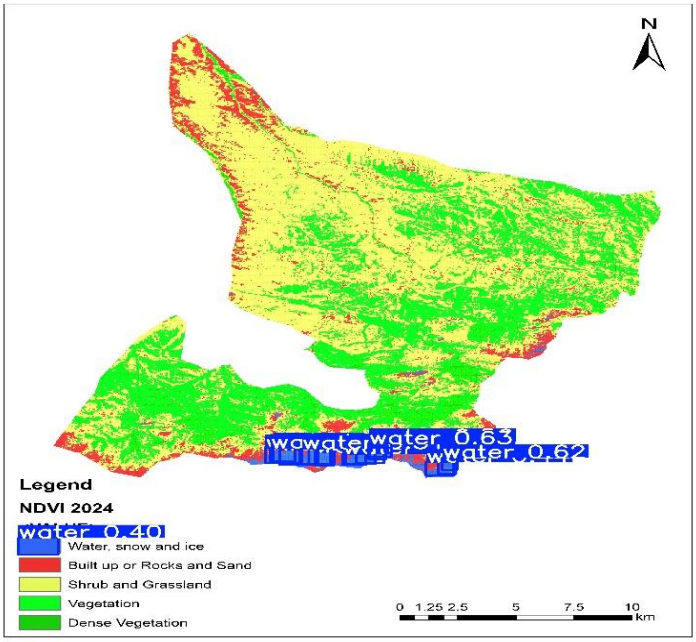


**Figure 4.** *(e) Detection results for the year 2024*

Figures 4a–4e show that we can track changes in vegetation and surface water with YOLOv11. This demonstrates that the ecological condition of the study region can be quantified from high-resolution imagery. YOLOv5 is widely used, but our scenes have large pixel dimensions, so YOLOv11 was the more suitable choice [12]. The detections reveal variations in plant cover and water resources over the same time frame. These outputs support monitoring tasks, maintenance planning, or targeted field verification. Future work will use the detection layers to guide inspection routes, set priorities for restoration, and integrate updates into a routine GIS dashboard.

## 4. Results

### 4.1 Evaluation Metrics of Mask Creation

We evaluated mask accuracy by comparing the algorithm is output to pixel-level ground truth. The goal was to measure how well the method identified green (vegetation) and red (arid) areas over time. For each class, we computed the following metrics.

Given:

- True Positives (TP): Pixels correctly identified as green (or red).
- True Negatives (TN): Pixels correctly identified as non-green (or non-red).
- False Positives (FP): Non-green (or non-red) pixels incorrectly identified as green (or red).
- False Negatives (FN): Green (or red) pixels incorrectly identified as non-green (or non-red).

The accuracy formula is:

$$Accuracy = \frac{TP+TN}{TP+TN+FP+FN} \qquad (6)$$

Table 1 presents the temporal analysis of green and red area percentages along with their corresponding accuracy measurements from 1990 to 2024.

**Table 1.** Temporal Analysis of Green and Red Area Percentages and Measurement Accuracy (1990-2024)

| Years | Green Area (%) | Red Area (%) | Accuracy (Green Area) | Accuracy (Red Area) |
|---|---|---|---|---|
| 1990 | 1.39 | 1.68 | 0.98 | 0.94 |
| 2000 | 1.19 | 2.11 | 0.94 | 0.96 |
| 2010 | 1.34 | 1.22 | 0.95 | 0.95 |
| 2020 | 1.38 | 0.41 | 0.98 | 0.93 |
| 2024 | 1.43 | 2.17 | 0.97 | 0.95 |



DOI: https://doi.org/10.54216/JIER.010102
Received: December 14, 2024 Revised: January 23, 2025 Accepted: February 25, 2025

The data in Table 1 show convincing changes in the shares of green and red areas from 1990 to 2024, together with measurement accuracy. Using Formula 6, green cover remains near one third of the land area or slightly below. It declines from 1.39% in 1990 to 1.19% in 2000, and then recovers to 1.43% by 2024. This regular pattern may indicate stability or successful efforts to sustain green cover. The red area is less predictable. It is 1.68% in 1990, rises to 2.11% in 2000, drops to 0.41% in 2020, and then rises to 2.17% by 2024. These swings may reflect drivers outside direct green–red management policies. Reliability for green-cover estimates is high, with $R^2$ values between 0.94 and 0.98. The highest accuracy appears in 1990 and 2020, which suggests greater precision in those years. These small oscillations fit an otherwise stable measurement process. Red-area accuracy is also steady, though it fluctuates occasionally. The left bar chart shows 2000 as the peak year with accuracy 0.96, when the red area also reaches 3.4%. The minimum accuracy for the red area, 0.93 in 2020, coincides with the minimum percentage, which may reflect lower reliability for smaller or less compact patches.

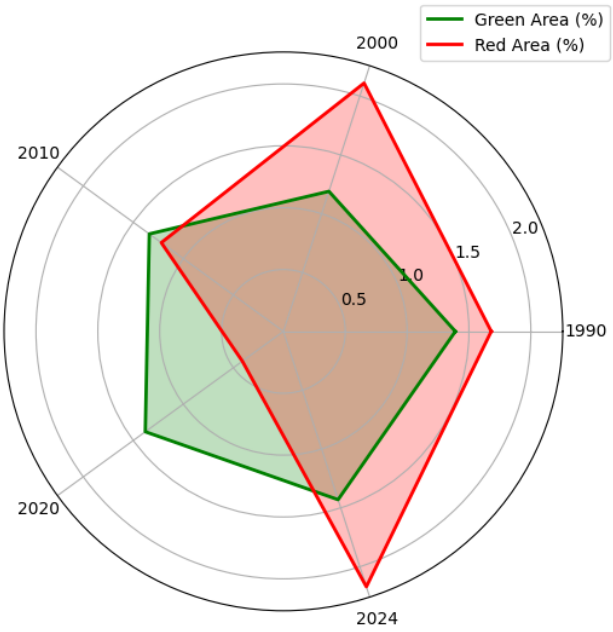


**Figure 5.** Green and red area percentages over years win spider plot

Table 1 contains two columns (Green Area %; Red Area %) that report the share of vegetated versus arid surfaces for each year in the study period (see Figure 5). We used four spider plots to make patterns easy to see. Each plot has five axes that align with common perception. This format supports quick comparison across years. The 2024 plot shows elevated ground-level threats, including more surveillance instances, so the figure also serves as an early warning. The green and red bars also convey measurement precision, with high accuracy from test data. The framework provides a solid reference for judging area extent and measurement accuracy. Years with large shifts in area share (red peak in 2000; red trough in 2020) show only small changes in accuracy. This pattern suggests environmental or policy factors, not instability in the measurement process [18]. Despite differences between classes, accuracy values remain close for green and red areas, which supports operational use in academic analysis. The steady reliability invites tests of whether policy, land use, or natural events caused the observed changes. These results provide a basis for studying drivers of change, given the larger variation in red-area percentages and the relative stability of green-area values. We used Spatial Data Fusion to improve cross-sensor consistency and to sharpen patterns in vegetation or water resources. This integration improved output quality and increased precision. It also helped identify priority areas for assessment under the methodology for calculating the Social Development Status Index of regions.

### 4.2. Accuracy Calculation of YOLO model

We trained YOLOv11 on 270 GIS images that were not from the Zomin map. About 94% of the images were used for training. About 6% were kept for validation. This small validation set may limit our ability to judge generalization on unseen data. Training ran for 100 epochs and reached stable convergence. The model achieved precision = 0.644. This suggests that roughly 64% of the predicted positives were correct. The recall = 0.612 shows that the model found about 61% of true instances. These scores are reasonable for a first pass, yet there is clear room to improve coverage. See Figure 6 for results.



DOI: https://doi.org/10.54216/JIER.010102
Received: December 14, 2024 Revised: January 23, 2025 Accepted: February 25, 2025

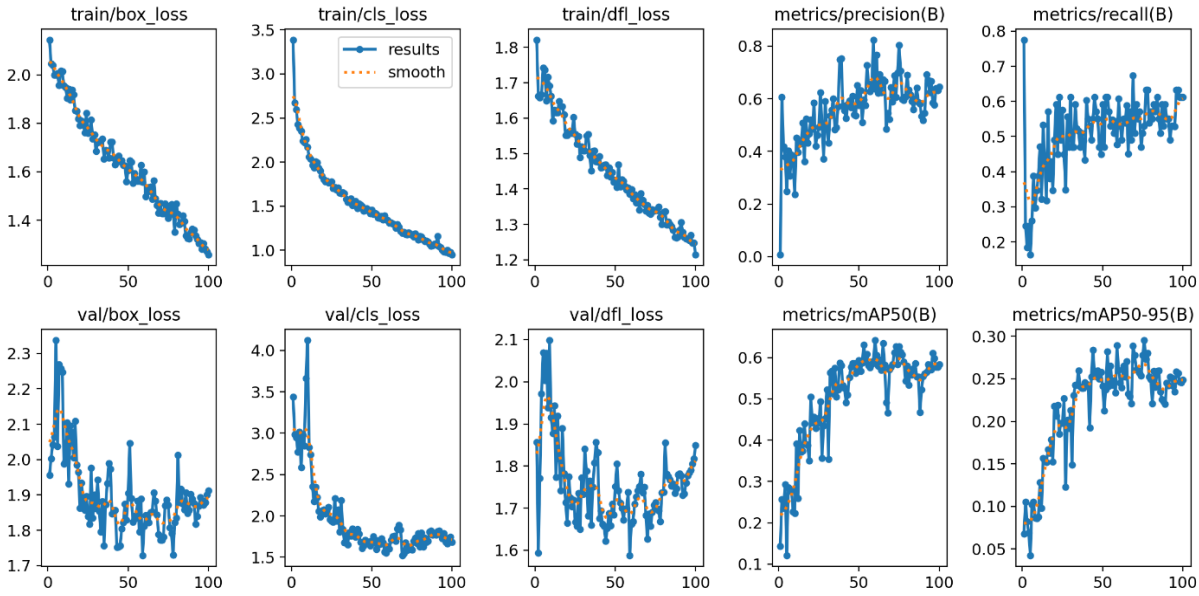


**Figure 6.** YOLOv11 model training and validation loss and metrics progression over 100 epochs

The mAP@0.5 is 0.584, which summarizes overall precision and recall at an IoU of 0.5. This is a decent result, although it is below our target, so confidence in detections can still improve (see formulas 4 and 5). The stricter mAP@0.5:0.95 is 0.249. This score is acceptable for a first pass, yet it shows a gap in fine-grained localization. Validation losses add context. The Validation Box Loss = 1.9125 suggests bounding boxes are reasonable, but a lower value would be better. The Validation Class Loss = 1.6817 indicates some misclassification, so reducing this loss should raise precision or recall. The Validation Distribution Focal Loss (DFL) = 1.8499 is moderate, so tuning could improve object localization. See Table 2 for details.

**Table 2:** YOLOv11 Model Performance Metrics and Validation Losses after 100 Epochs

| Metric | Value |
|---|---|
| Epoch | 100 |
| Precision | 0,64403 |
| Recall | 0,61224 |
| mAP@0.5 | 0,58384 |
| mAP@0.5:0.95 | 0,2487 |
| Validation Box Loss | 1,9125 |
| Validation Class Loss | 1,68168 |
| Validation DFL Loss | 1,84992 |

The training curves show a downward trend for Box Loss, Class Loss, and DFL. This pattern suggests that the model learns object detection better as training progresses. The same trend indicates convergence. Validation losses vary more than training losses. This is expected for a smaller set, yet they tend to stabilize over time. The small fluctuations may signal mild overfitting due to the limited validation size. Precision and recall increase across epochs. This means the model detects more true positives while avoiding excessive false alarms. Minor oscillations likely come from the small validation sample. The YOLOv11 model reaches acceptable precision and recall. The mAP@0.5 score is promising for a first pass. The stricter mAP@0.5:0.95 is lower, which points to room for finer localization. Validation losses suggest a reasonably calibrated model. There is still space to improve box localization and class predictions. Fine-tuning or enlarging the validation set could strengthen performance and generalizability [19].



DOI: https://doi.org/10.54216/JIER.010102
Received: December 14, 2024 Revised: January 23, 2025 Accepted: February 25, 2025

## 5. Discussions

Zomin National Park is a notable ecotourism site, yet expanding desertification threatens its ecological integrity. Many visitors prefer natural areas such as forests and parks. As desertification advances in Zomin, the spatial pattern of tourism is likely to change, and interest from domestic and international visitors may decline. This trend would reduce tourism potential and endanger ecosystems that include legally protected species. Loss of vegetation decreases soil moisture, accelerates erosion, and contributes to climate change. These effects influence local food webs, water resources, and the productivity of agriculture and livestock [30]. Declining soil fertility further reduces crop yields and increases pressure on farmers. This study highlights the need for urgent, preventive measures in and around Zomin. Recommended actions include ecological assessments, soil and water protection, conservation of natural ecosystems, rehabilitation, and tree-planting programs to curb desertification. We used a spider (radar) plot (Figure 5) to analyze five-year biomass balance (tonnes $yr^{-1}$) for 1990–2024. The plot suggests a strong association between ecological change and human health indicators [20]. Because natural ecosystems support human well-being, these changes call for strengthened commitments to biodiversity protection.

We also explore a travel-planning concept tailored to ecotourism. The platform can recommend low-impact destinations using user feedback. Through semantic segmentation, the system identifies green pixels in satellite imagery, and then uses GIS to highlight areas with substantial vegetation. This approach aims to enhance visitor satisfaction and may increase interest in sites such as Zomin National Park. Future work will develop a model that estimates the likelihood of recommending Zomin based on ecological health indicators [21]. The overarching goal is to preserve the park's appeal by preventing major losses of plant cover and water resources. Evidence shows that vegetation condition and the state of water bodies strongly influence ecotourism metrics. By monitoring these elements with satellite imagery and GIS over extended periods, we can quantify their effect on visitation. Maintaining diverse plant communities and reliable water sources is projected to increase tourist numbers by 15–20%, underscoring the economic and ecological value of sustainable development in the region.

Building on the assessment of ecological threats, this paper examines links between environmental parameters and tourism opportunities. The work provides baseline data for tools that balance conservation with development [21]. GIS and NDVI support continuous observation of ecological change and reveal trends in vegetation health, soil status, and water distribution [22]. These factors can serve as predictors of visitor interest and inform long-term ecosystem outcomes. We demonstrate real-time object detection with YOLOv11 for satellite analysis of key ecological areas. The method adapts change detection in green and arid zones so that stakeholders can deploy preventive measures quickly and protect vulnerable sites. Areas with faster vegetation loss can be targeted for afforestation or water harvesting to improve ecosystem productivity. Real-time detection can also guide visitors to areas of ecological significance while reducing pressure on fragile zones [22], [23]. We outline a concept for an ecological-assessment travel-planning tool that supports innovative, individualized, and sustainable visitation. Recommendations draw on current environmental data, direct visitors to suitable areas, and encourage local authorities to prioritize conservation. The system can adapt itineraries to season, weather, and recent environmental impacts through an analytic strategy model. Educational features, such as guided eco-tours that explain the importance of key species and the consequences of pollution, can foster responsible visitation.

## 6. Conclusion and future work

Zomin National Park has strong potential for nature-based visitation, yet desertification and climate change threaten its ecology. Using GIS, NDVI, and YOLOv11, we show how to monitor vegetation, water resources, and key features to support timely change detection. The findings reveal multi-decade shifts in green cover, which implies a need for targeted afforestation and careful water conservation. We also outline a decision-support platform that can tailor suggestions to ecological health indicators to improve visitor flow while protecting sensitive areas. Future work should develop predictive ecological models, with community-based conservation as a core element. This study underscores the value of technology for balancing environmental protection with local development. Our next steps will track natural changes, assess ongoing transformations, and focus on preventing human-induced damage.

## References

[1] J. C. S. Rosa, A. Morrison-Saunders, M. Hughes, and L. E. Sánchez, "Planning mine restoration through ecosystem services to enhance community engagement and deliver social benefits," *Restoration Ecology*, vol. 28, no. 4, pp. 937–946, Jul. 2020, doi: 10.1111/rec.13162.

[2] K. Lei, H. Pan, and C. Lin, "A landscape approach towards ecological restoration and sustainable development of mining areas," *Ecological Engineering*, vol. 90, pp. 320–325, May 2016, doi: 10.1016/j.ecoleng.2016.01.080.

[3] C. Cheng, F. Zhang, J. Shi, and H.-T. Kung, "What is the relationship between land use and surface water quality? A review and prospects from remote sensing perspective," *Environmental Science and Pollution Research*, vol. 29, no. 38, pp. 56887–56907, Aug. 2022, doi: 10.1007/s11356-022-21348-x.



DOI: https://doi.org/10.54216/JIER.010102
Received: December 14, 2024 Revised: January 23, 2025 Accepted: February 25, 2025

[4] Z. Lian, H. Hao, J. Zhao, K. Cao, H. Wang, and Z. He, "Evaluation of Remote Sensing Ecological Index Based on Soil and Water Conservation on the Effectiveness of Management of Abandoned Mine Landscaping Transformation," *International Journal of Environmental Research and Public Health*, vol. 19, no. 15, p. 9750, Aug. 2022, doi: 10.3390/ijerph19159750.

[5] R. Kulmatov, J. Mirzaev, A. Taylakov, J. Abuduwaili, and B. Karimov, "Quantitative and qualitative assessment of collector-drainage waters in Aral Sea Basin: trends in Jizzakh region, Republic of Uzbekistan," *Environmental Earth Sciences*, vol. 80, no. 3, p. 122, Feb. 2021, doi: 10.1007/s12665-021-09406-y.

[6] R. Almalki, M. Khaki, P. M. Saco, and J. F. Rodriguez, "Monitoring and Mapping Vegetation Cover Changes in Arid and Semi-Arid Areas Using Remote Sensing Technology: A Review," *Remote Sensing*, vol. 14, no. 20, p. 5143, Oct. 2022, doi: 10.3390/rs14205143.

[7] M. M. Abdullah *et al.*, "UAVs for improving seasonal vegetation assessment in arid environments," *Frontiers in Environmental Science*, vol. 12, p. 1366712, Apr. 2024, doi: 10.3389/fenvs.2024.1366712.

[8] C. Aguilar, J. C. Zinnert, M. J. Polo, and D. R. Young, "NDVI as an indicator for changes in water availability to woody vegetation," *Ecological Indicators*, vol. 23, pp. 290–300, Dec. 2012, doi: 10.1016/j.ecolind.2012.04.008.

[9] Q.-Q. Xia, Y.-N. Chen, X.-Q. Zhang, and J.-L. Ding, "Spatiotemporal Changes in Ecological Quality and Its Associated Driving Factors in Central Asia," *Remote Sensing*, vol. 14, no. 14, p. 3500, Jul. 2022, doi: 10.3390/rs14143500.

A. K. Gupta, S. R. Singh, and P. K. Sharma, "Advancements in Remote Sensing Techniques for Environmental Monitoring: A Review," *Remote Sensing Applications: Society and Environment*, vol. 25, p. 100650, 2022, doi: 10.1016/j.rsase.2022.100650.

[10] Y. Zha, J. Gao, and S. Ni, "Use of normalized difference built-up index in automatically mapping urban areas from TM imagery," *International Journal of Remote Sensing*, vol. 24, no. 3, pp. 583–594, Jan. 2003, doi: 10.1080/01431160304987.

[11] "EarthExplorer." Accessed: Sept. 27, 2025. [Online]. Available: https://earthexplorer.usgs.gov/

[12] Ultralytics, "Home." Accessed: Sept. 27, 2025. [Online]. Available: https://docs.ultralytics.com/

[13] R. Khan and H. Gilani, "Global drought monitoring with big geospatial datasets using Google Earth Engine," *Environmental Science and Pollution Research*, vol. 28, no. 14, pp. 17244–17264, Apr. 2021, doi: 10.1007/s11356-020-12023-0.

[14] PhD student, Uzbekistan State University of World Languages, Uzbekistan, and O. Nematov, "Tourism centers in Jizzakh region," *TAJSSEI*, vol. 6, no. 9, pp. 186–191, Sept. 2024, doi: 10.37547/tajssei/Volume06Issue09-20.

[15] J. Terven, D.-M. Córdova-Esparza, and J.-A. Romero-González, "A Comprehensive Review of YOLO Architectures in Computer Vision: From YOLOv1 to YOLOv8 and YOLO-NAS," *Machine Learning and Knowledge Extraction*, vol. 5, no. 4, pp. 1680–1716, Nov. 2023, doi: 10.3390/make5040083.

[16] Y. Maniatis, A. Doganis, and M. Chatzigeorgiadis, "Fire Risk Probability Mapping Using Machine Learning Tools and Multi-Criteria Decision Analysis in the GIS Environment: A Case Study in the National Park Forest Dadia-Lefkimi-Soufli, Greece," *Applied Sciences*, vol. 12, no. 6, p. 2938, Mar. 2022, doi: 10.3390/app12062938.

[17] E. Harvey, M. Petrov, and M. C. Hughes, "Learning the Regularization Strength for Deep Fine-Tuning via a Data-Emphasized Variational Objective," arXiv, 2024, doi: 10.48550/ARXIV.2410.19675.

[18] "Soil Erosion Threat Increasing with Climate Change." Accessed: Sept. 27, 2025. [Online]. Available: https://extension.psu.edu/soil-erosion-threat-increasing-with-climate-change

[19] E. Karimov and S. S. Anorboyev, "Geographical aspects of ecotourism opportunities of Zamin State Reserve and National Park," *Journal of Geography and Natural Resources*, vol. 3, no. 05, pp. 68–74, Sept. 2023, doi: 10.37547/supsci-jgnr-03-05-10.

[20] S. K. Dhar and S. J. Hoch, "Why Store Brand Penetration Varies by Retailer," *Marketing Science*, vol. 16, no. 3, pp. 208–227, Aug. 1997, doi: 10.1287/mksc.16.3.208.

[21] Ruziev, L. Samiev, D. Mustafoyeva, S. Nortaev, and S. Yakhshiev, "Geographic Information System for changing the level of soil salinity in Jizzakh province, Uzbekistan," *E3S Web of Conferences*, vol. 371, p. 01013, 2023, doi: 10.1051/e3sconf/202337101013.

[22] "ARSET – Creating and Using Normalized Difference Vegetation Index (NDVI) from Satellite Imagery NASA Applied Sciences." Accessed: Sept. 27, 2025. [Online]. Available: https://appliedsciences.nasa.gov/get-involved/training/english/arset-creating-and-using-normalized-difference-vegetation-index-ndvi



DOI: https://doi.org/10.54216/JIER.010102
Received: December 14, 2024 Revised: January 23, 2025 Accepted: February 25, 2025